Energy 185 (2019) 463–476

Contents lists available at ScienceDirect

Energy

journal homepage: www.elsevier.com/locate/energy

Energy, exergy and environmental analysis of a hybrid combined cooling heating and power system integrated with compound parabolic concentrated-photovoltaic thermal solar collectors

Jiangjiang Wang [a, b, *], Yuzhu Chen [a], Noam Lior [b], Weihua Li [a]

[a] School of Energy, Power and Mechanical Engineering, North China Electric Power University, Baoding, Hebei Province, 071003, China
[b] Department of Mechanical Engineering and Applied Mechanics, University of Pennsylvania, Philadelphia, PA 19104, USA

ARTICLE INFO

Article history:
Received 13 March 2019
Received in revised form
3 June 2019
Accepted 3 July 2019
Available online 11 July 2019

Keywords:
Combined cooling heating and power (CCHP) system
Compound parabolic concentrators (CPC)
Photovoltaic-thermal (PVT)
Thermodynamic performance
Environmental benefits

ABSTRACT

The objective of this paper is to propose and analyze the performance of a novel hybrid combined cooling heating and power (CCHP) system coupled with compound parabolic concentrator-photovoltaic thermal (CPC-PVT) collectors. The electricity and hot water from CPC-PVT are integrated with the electricity and waste heat carried by exhaust gas and jacket water from the internal combustion engine to improve the energy performance. The thermodynamic models were constructed and validated by comparing the simulation results to those from existing studies. The thermodynamic performances were analyzed and the impacts of key parameters on the performances were discussed at the off-design condition. The levelized primary energy saving ratio (PESR) and carbon dioxide emission reduction ratio (CDERR) of the hybrid CCHP system in comparison to the CCHP system without solar energy were employed to evaluate the contribution of solar energy. The results indicated that the energy and exergy efficiencies at the design condition are 63.3% and 21.8% in summer, respectively, and 61.8% and 27.1% in winter, respectively. Compared to the CCHP system without solar energy, the hybrid system has more flexible ability to adjust the heating to electricity ratio and achieves the maximum levelized PESR of 28.6% and CDERR of 36.7%, respectively.

1. Introduction

Distributed energy systems (DESs) including combined heat and power (CHP) systems and combined cooling heating and power (CCHP) systems, which encompass varieties methods of electricity generation, energy storage and conversion, and system control solutions, have become more attractive in recent years owing to their high overall energy utilization efficiency and flexible operation strategies [1,2]. Furthermore, to reduce fuel consumption and emissions and satisfy energy sustainability requirements, hybrid DES systems driven by natural gas in combination with renewable energy resources, which focused mostly on integrated conceptual designs [3], theoretical studies [4], system configurations and parameters optimization [5], and exergoeconomic analysis [6,7], become more popular to scholars. Among the renewable energy resources, solar energy appears currently to be one of the most promising alternatives for research because of its friendly performances in environment and economy.

The concept of hybrid thermal system was early proposed and developed, such as hybrid solar powered/fuel assisted steam cycles [8–11]. Solar energy is transformed to other energy forms for users through solar heat collectors and photovoltaic (PV) panels. The solar heat collectors include non-concentrating (stationary) and concentrating tracking ones for heating fluids to different temperatures by absorbing the solar irradiance, while the PV module can directly convert the solar irradiance into electricity. The solar-assisted DESs include solar cooling system [12], CHP system coupled with PV devices [13,14], CCHP system integrated with solar collectors [15], CCHP system hybridized with PV panels and solar thermal collectors [16], parabolic trough collectors (PTC) driven organic Rankine cycle system [17], and CCHP system coupled with solar CPC or dish collectors [18,19]. Among these studies, the solar utilization applications integrated into CCHP systems included those that supply only heat and those that supply electricity by PV panels separately.

* Corresponding author. School of Energy, Power and Mechanical Engineering, North China Electric Power University, Baoding, Hebei Province, 071003, China.
E-mail address: wangjj@ncepu.edu.cn (J. Wang).

https://doi.org/10.1016/j.energy.2019.07.027
0360-5442/

Nomenclature

AHE	absorption heat exchanger
CCHP	combined cooling heating and power
CDE	carbon dioxide emission
CDERR	carbon dioxide emission reduction ratio
CHP	combined heat and power
COP	coefficient of performance
CPC	compound parabolic concentrators
FEL	following electrical load
FTL	following thermal load
HG	high-pressure generator
HX	heat exchanger
ICE	internal combustion engine
LG	low-pressure generator
LX	low temperature heat exchanger
PESR	primary energy saving ratio
PVT	photovoltaic-thermal (PVT) collectors
TES	thermal energy storage

Symbols

A_a	total aperture area for CPC-PVT, m^2
A_{rm}	area of receiver covered by PV module, m^2
c	specific heat, kJ/(kg·K)
cc	Carnot cycle
E	electricity, kW
Ex	exergy, kW
f_f	geometric factor
F_{TES}	surface area of TES, m^2
h	enthalpy, kW/kg
I_b	direct beam solar irradiance, W/m^2
m	mass, kg
Ne	nominal generation capacity, kW
K	average heat transfer coefficient, W/m^2 K
PF_1	heat transfer factor due to the glass covers of module
PF_2	heat transfer factor due to the plate below of module
PF_c	heat transfer factor due to the glass covers for the glazed portion
Q	energy, kW
T	temperature, °C
U_{Lc}	overall heat transfer coefficient from glassing to ambient ($W/(m^2 \cdot K)$)
$U_{l,m}$	overall heat transfer coefficient from module to ambient ($W/(m^2 \cdot K)$)
$U_{tc,a}$	overall heat transfer coefficient from cell to ambient ($W/(m^2 \cdot K)$)
$U_{tc,p}$	overall heat transfer coefficient from cell to plate ($W/(m^2 \cdot K)$)
$U_{tp,a}$	overall heat transfer coefficient from plate to ambient ($W/(m^2 \cdot K)$)
w	concentration of LiBr solution
η	efficiency
β_0	temperature coefficient of efficiency
β_c	efficiency of CPC
τ_g	transmissivity of glass
γ	electricity generation efficiency based on a natural gas plant
ρ	density of hot water, kg/m^3
α_P	absorptance of absorber plate

Subscripts

a	ambient
au	auxiliary
c	solar cell
$cool$	chilled water
dom	domestic hot water
exh	exhaust gas
f	fluid water
$heat$	space heating water
i	inlet
jac	jacket water
m	PV module
ng	natural gas
o	outlet
ph	physical
ref	reference CCHP system
sol	solar energy
sys	hybrid system
sun	sun
0	standard reference state

Compared to the integration of solar PV panels or solar heat collectors separately in such systems, the flat plate photovoltaic thermal (PVT) solar system and concentrating parabolic PVT (CPVT) system, which integrate the PV cells into a solar heat collector, can convert solar irradiance to heat and electricity simultaneously. The two products from these collectors can be easily combined to CCHP systems [20,21], and the integration can raise the ratio of electricity to heat supply of the CCHP system. This breaks the fixed ratio limitation of conventional CCHP systems in following electrical or thermal load modes [22] that often result in the excess or shortage of the systems' products when users' loads vary.

The PVT system consists of two main parts: solar PV cells to convert the solar irradiance into electricity, and solar heat collectors on the back of the PV panels to cool the PV panels and thereby also collect useable heat. This configuration of the PV panels not only increases overall system efficiency because of the simultaneous generation of heat and electricity, but also increases their operational efficiency and prolongs their life. The typical PVT is the integration of the heat collectors into a flat plate PV panel. The cooling fluids are typically air and water for different applications and purposes. For example, the PVT air heater system [23] can be self-sustainable and feasible for preheating air for other utilizations, and the PVT water collector [24] can produce hot water for users on the base of power generation. This integration of the PVT flat plate collector has higher overall energy efficiency and uses much less space than the separately-installed PV module and solar thermal collector [24]. Aiming to further improve solar energy utilization efficiency, the compound parabolic concentrator (CPC) PVT system which coupled the CPC reflectors with basic flat plate PVT system was proposed and developed, and the investment cost of unit energy could be lower than the cost of the typical PVT collectors at the same solar irradiance, and the concentrated PVT system produces solar hot water (or other fluid) with higher temperature [25]. It was reported in Ref. [25] that a series-connected partially covered (25%) CPC-PVT collector produces hot water of 190 °C, thus increasing the heat applications potential. Moreover, the comparisons between CPC-PVT system and flat plate PVT in Refs. [26–28] demonstrated the advantages of CPC-PVT in installation areas, energy and exergy performances, overall CO_2 reduction and primary energy saving potentials. The maximal thermal efficiency of CPC-PVT (34%) was about 2 times as much as the flat plate PVT system [26]. The electricity and thermal outputs of CPC-

PVT were 3 and 2 times more than the outputs of flat plate PVT, respectively [28]. The CPC reflector effectively improve solar energy utilization. To optimize the structures and improve efficiency, various aspects of CPC-PVT including solar materials [32], modeling [30], structure optimization [31], and performance evaluations of energy outputs [28] or thermodynamic efficiencies [27] were studied.

The progress of CPC-PVT technologies also promotes the proposal and development of novel and advanced power systems [33]. Using the electricity and heat from PVT to supply energy to other system components, a self-sustained vapor absorption refrigeration system was proposed [34] for which CPC-PVT system was stated to be the most appropriate one through comparing to other types of PVT. A multi-effect evaporation desalination system coupled with concentrating PVT collectors [35] can operate over a wide range of temperatures that can enable the utilization of more sophisticated and more efficient desalination with thermal vapor compression or absorption vapor compression. A few works studied the CCHP system based on concentrating PVT collectors. A concentrating dish PVT system in the study of [21] was designed and developed to produce electricity, space heating, cooling and domestic hot water, and the results through modeling and simulation indicated that it can operate all year long with great potentials in cost reduction and energy saving. The simulation and application of a CCHP system based on concentrating parabolic trough PVT in a hospital [20] indicated that it achieved better performance and was profitable without any public funding. These two systems just utilize solar energy, not hybrid system. Few hybrid CCHP systems integrated with the CPC-PVT were proposed and developed. Compared to the CCHP system in Refs. [20,21], the proposed novel system in this paper has the following obvious differences: (1) The CCHP system is a hybrid system driven by natural gas and solar energy, which can operate all year long, even without solar irradiance. (2) The CPC-PVT adopts the low concentrating ratio collector, which occupies less land and investment cost could be low.

In this study, a new hybrid CCHP integrated with CPC-PVT solar collectors is investigated. The contributions of this work include: (1) A novel hybrid CCHP system based on CPC-PVT solar collectors is proposed for effective utilization of solar energy in the conventional natural gas CCHP system. The energy flowcharts are determined based on the energy cascading utilization and an effective integrated utilization of renewable energies can be achieved. (2) The thermodynamic models are constructed, and the waste heat utilization, energy and exergy performances in the different operation modes are obtained after the validations of subsystems. The impacts of key parameters on system performances in variable conditions are investigated and compared with other relevant studies. (3) The criterion of levelized primary energy saving ratio of the hybrid system in comparison to natural gas CCHP system is proposed and defined to consider the difference of energy grades. Compared to the conventional CCHP system without solar energy, the energy and emission benefits achieved by the hybrid system are evaluated based on the annual dynamic operating.

2. System description

The energy flowcharts of the hybrid CCHP system integrated with CPC-PVT are displayed in Fig. 1. The integrated system includes an internal combustion engine (ICE) subsystem, a CPC-PVT subsystem, an absorption heat exchanger (AHE) subsystem, and a thermal energy storage (TES) subsystem.

Natural gas (state 1) with air (state 2) is combusted in the ICE to generate electricity (state 3); subsequently, the waste heat in two forms including exhaust gas (state 6) and jacket water (state 9) is recovered by the latter waste heat utilization subsystem. The CPC-PVT subsystem converts solar irradiance to electricity (state 4) and thermal energy that heats the cooling water (state 10) and produces solar hot water (state 11) simultaneously. The total electricity (state 5) from the ICE (state 3) and CPC-PVT (state 4) is sent to the building. When excess or shortage of electricity occurs, it should be sent to the grid (state E2) or taken from it (state E1), respectively.

The waste heat from the ICE and CPC-PVT includes three sources with different temperatures: exhaust gas (state 6), jacket water (state 9) from the ICE, and solar hot water (state 11) from the CPC-PVT. According to their temperatures, the exhaust gas (state 6) from ICE of which the temperature is approximately 470 °C is fed to the high-pressure generator (HG) of the AHE. The outlet exhaust gas (state 7) at 170 °C from the AHE adds heat in HX2 to heat the solar hot water (state 11) coming from the CPC-PVT. Finally, the exhaust gas exits to the environment (state 8) at 120 °C. The jacket water from the ICE at 85 °C (state 9), and the heated hot water from the CPC-PVT and HX2 (state 12) is mixed together (state 13) to generate the chilled water (states a6 and a5) or space heating water (states a3 and a4).

(1) The cooling operation condition

At the cooling operation condition, the AHE is used to produce chilled water (state a6) for space cooling and domestic hot water (state a2). It consists of high-pressure generator (HG), two low pressure generators (LG1 and LG2), heat exchanger (HX1), low temperature heat exchanger (LX), high temperature heat exchanger (HX), throttle, condenser, absorber and evaporator. During its operation, the valves of V4 and V9 are closed while others are open to control the fluid flow. The weak solution (state b1) is preheated in LX (state b2) by absorbing the heat from strong solution (state b3), then split into two parts (states b2" and b2′). After preheated in HX, one part of weak solution (state b5) flows to HG, where it absorbs the heat from exhaust gas (state 6) and generates the first part of refrigerant water steam (state b8) and strong solution (state b6). Another part of weak solution (state b2") goes to LG1 to absorb the heat from mixed hot water (state 14) and generate the second part of refrigerant water steam (state b11") and strong solution (state b10). The strong solution (state b6) which releases heat in HX (state b7), mixes with the strong solution from LG1 (state b10) and flows to LG2. The first part of the refrigerant steam (state b8) from HG is then split into two parts (states b9″, b9′), where the one (state b9") flows to LG2 and releases the heat, while the mixed solution which comes from LG1 (stage b10) and HX (stage b7), absorbs the heat and generates the third part of steam (state b11′) and strong solution (state b3). The other part of the refrigerant (state b9′) is used to generate domestic hot water (state a2) in HX1 by releasing the heat to tap water (state a1). The strong solution (state b3) from LG2 flows to the absorber (A) after releasing heat to weak solution (state b1) in LX. Three parts of refrigerant water from HG (state b9), LG1 (state b11″) and LG2 (state b11′) are condensed by cooling water in the condenser (C). The low-pressure and low-temperature refrigerant (state b12′) flows into the evaporator after a throttling process. In the evaporator, the liquid refrigerant (state b12′) by taking heat from the chilled water is evaporated and then the refrigerant vapor (state b13) is taken by the strong solution (state b4) in absorber (A). Moreover, the cooling water (state a7) is needed to decrease the absorber's temperature.

When there is no excess waste heat, the valves, Va1 to Va9, and Va12, are closed while other valves are open. Both the heat from exhaust gas (state 6) and the mixed hot water (state 13) drives the AHE. Otherwise, the valves Va1 and Va2 are open and the excess heat is stored into the TES tank (states 21, 22). When the waste heat from the ICE and CPC-PVT is insufficient, the valves Va3 and Va4 are open and the stored heat in the TES tank is used to supplement the

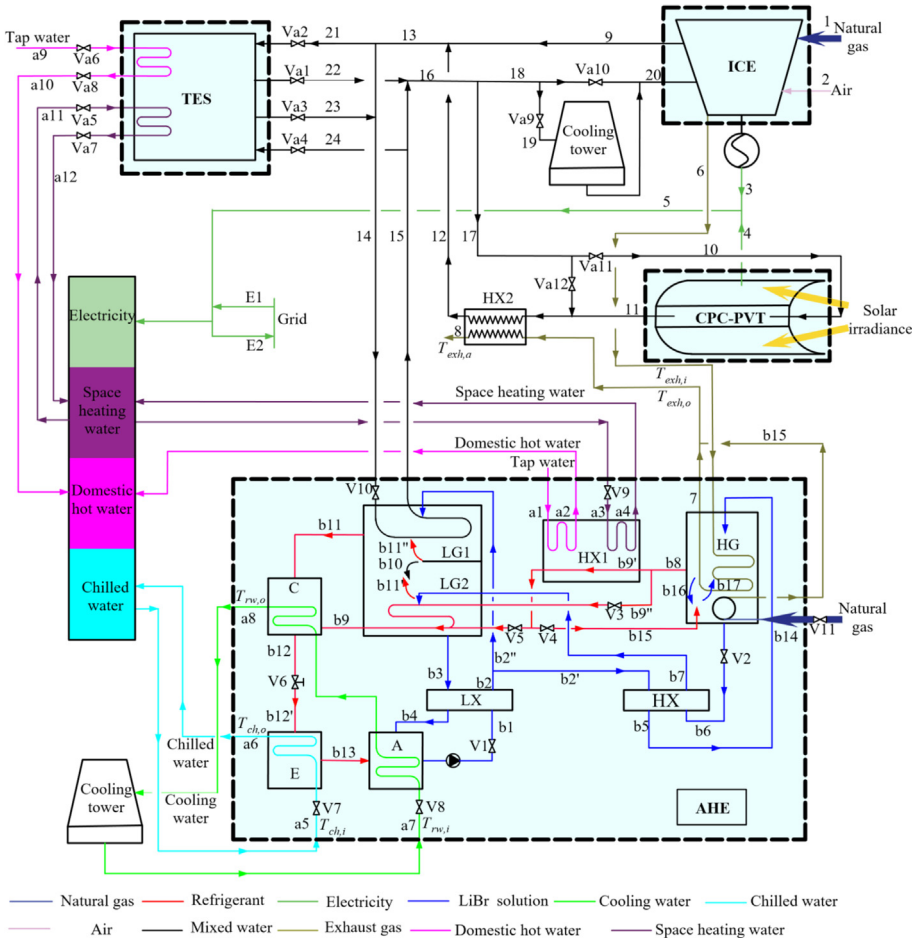

Fig. 1. Energy flowchart of the hybrid CCHP system integrated with CPC-PVT.

shortage (states 23, 24).

After releasing heat, the hot water (state 16) is divided into two parts (states 17 and 18). One part (state 17) returns to CPC-PVT and HX2 for the next cycle, while the other part (state 18) is returned to the jacket of the ICE. When there is no solar irradiance, the hot water (state 17) will be sent to HX2 directly by opening valve Va12 and closing valve Va11. To satisfy the temperature requirement of jacket water, the hot water (state 18) flows to the cooling tower to be cooled when its temperature is higher than the setting temperature, by opening valve V9 and closing V10.

As for the domestic hot water, the shortage is supplemented (states a9, a10) by opening valves Va6 and Va8 when its demand is larger than the production in AHE (state a2). If all the recovered heat from ICE, CPC-PVT and TES cannot fulfill the cooling or domestic hot water demand, the valve V11 is open and natural gas (state b14) is combusted in the HG to generate more heat.

(2) The heating operation condition

The AHE operates as a heat exchanger and only the HG and HX2 work in the heating operation condition. The valves of V4 and V9 are open while others are closed. The weak solution (state b17) in HG absorbs the heat from exhaust gas (state 6) and generates the refrigerant vapor (stage b8) and strong solution (stage b16). Due to the higher density, the strong solution (stage b16) flows downward in HG, while the refrigerant vapor (stage b8) releases the heat in HX1 to generate space heating water (state a4) and domestic hot water (state a2). The refrigerant water (stage b15) is then absorbed by the strong solution (stage b16) in the lower part of the HG, for the next cycle.

The mixed hot water (state 13) from ICE (state 9), CPC-PVT and HX (state 12) is directly fed to the TES tank by opening valves Va1 and Va2 in the heating condition. When the space heating or domestic hot water demands cannot meet by the AHE, the valves Va5 and Va8 or Va6 and Va7 are opened, and the TES tank supplies the shortages during the heating condition. Additionally, when the recovered heat cannot fulfill the building demands, the operation states and strategies are similar to the ones on the cooling operation condition.

From the analysis of energy flows, it is observed that the integration is relatively complex and there are some parameters to be adjusted or controlled for cost-efficient operation. For example, the temperature of solar hot water must match the temperature of jacket water. But it is easily and greatly influenced by the solar irradiance and ambient temperature. An intelligent control system is needed for adjusting the temperature of solar hot water according to weather parameters. When switching operation modes for user's demands, an appropriate control strategy is needed for controlling the valves to guarantee safe operation and energy-efficient supply. It is noted that the required somewhat complex controls slightly raise the system costs, which are, however, estimated to be significantly lower than the hybrid's operating energetic benefits.

3. The thermodynamic models

3.1. CPC-PVT

The structure of the considered CPC-PVT solar collector is shown in Fig. 2 and the basic structural parameters of single collector are listed in Table 1 [25], while the entire collector system is constructed in a series-parallel flow configuration to achieve similar temperatures of the solar and engine jacket hot waters. In the PVT, 25% lower area of collector is covered by a PV module while the remaining area is covered by (transparent) glass. The PV module converts the solar irradiance to electricity. Water flows through the lower level of the collector adjacent to the PV-covered inlet part and then adjacent to the glazed part. The water inlet temperature is T_{fi}, rising to the outlet T_{fom} and (see Fig. 2) T_{fo}.

To simplify the complex heat transfer model to focus on the output of electricity and hot water, the following assumptions are made in the modeling [32]: 1) The system is at steady state, 2) Ohmic losses in the PV module are ignored, 3) The heat capacities of glass cover, insulation, solar cell, and absorber, are ignored, and 4) The temperature gradients across the thickness of the PV module, insulation, and covered glass are ignored [36]. The validation of modeling was checked in section 5.1 before using these models. The energy balances of the solar cell, the absorber plate below the PV module, and the flowing water under the absorber plate can be expressed according to the heat transfer and the detailed equations can be found in Refs. [32,37].

The useful thermal energy, $Q_{sol,en}$, gained by the partially CPC-PVT collector are calculated respectively [38].

$$Q_{sol,en} = m_f c_f \left(T_{fo} - T_{fi}\right) \tag{1}$$

Exergy or second law analysis is a powerful tool to investigate the different energy converting systems in order to clarify the main source of irreversibility. It is conducted because it assigns equitable

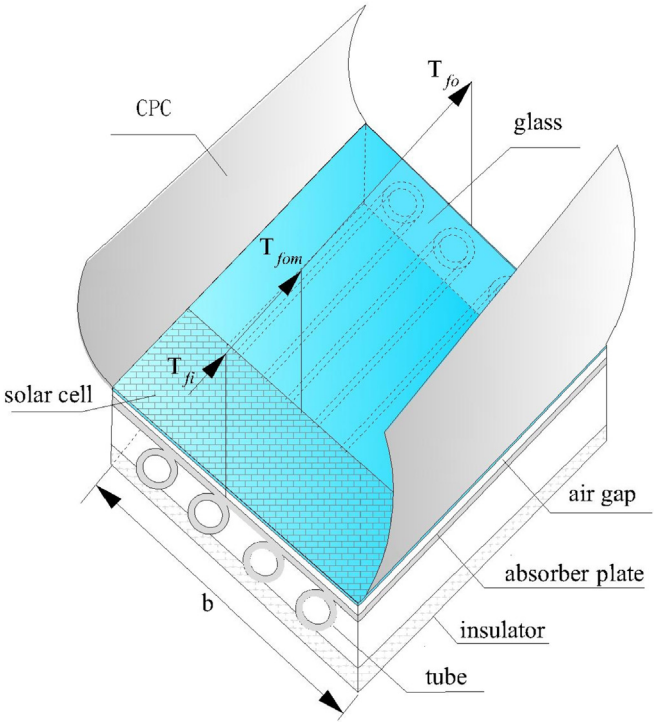

Fig. 2. Structure view of partially covered CPC-PVT [36].

Table 1
Parameters of the partially covered CPC-PVT collector [32] (their definitions are included in the Nomenclature).

Parameter	Value	Parameter	Values	Parameter	Value
A_a	2 m^2	A_{am}	0.5 m^2	A_{rm}	0.25 m^2
A_{ac}	1.5 m^2	A_{rc}	0.75 m^2	A_r	1 m^2
ρ	0.84	τ_g	0.95	α_c	0.9
β_c	0.88	α_P	0.8	F'	0.9680
K_g	0.816 W/m K	L_g	0.003 m	L_i	0.100 m
K_i	0.166 W/m K	K_P	6 W/m K	L_P	0.002 m
FF	0.8	η_0	0.209	h_{pf}	100 W/m k
h_i	5.7 W/m K	D_0	0.0125 m		

weight to the heat and work sources and products in this system, allows examination of the CPC-PVT on the exergy efficiency of the hybrid system, and presents design and optimization guidance for minimizing the components and system irreversible losses.

The physical exergy of hot water, Ex_{ph}, without the explicit consideration of the drop of pressure in a constant temperature-averaged specific heat, is calculated by eq. (2) [39].

$$Ex_{ph} = mc\left(T - T_0 - T_0 \ln\left(\frac{T}{T_0}\right)\right) \tag{2}$$

and the thermal exergy of the solar hot water, $Q_{sol,ex}$, is calculated by Ref. [38].

$$Q_{sol,ex} = m_f c_f \left(T_{fo} - T_{fi}\right) - m_f c_f (T_a + 273)\ln\frac{\left(T_{fo} + 273\right)}{T_{fi} + 273} \tag{3}$$

where m_f is the mass flow of the fluid water; c_f is the specific heat of water. T_{fi} and T_{fo} are the inlet and outlet fluid temperatures for CPC-PVT, respectively. T_a is the ambient temperature.

The time-changes of the solar irradiance incidence angle and intensity, as well as the ambient temperature, directly influence the efficiency of CPC-PVT, but this study focuses on thermodynamic effects and thus, for analysis simplification, the solar and ambient temperature are assumed to be at appropriate average steady state values.

The electrical efficiency of the CPC-PVT-collector solar cell η_c, can be expressed as [40].

$$\eta_c = \eta_0[1 - \beta_0(T_c - T_0)] \tag{4}$$

where T_c is the solar cell temperature; β_0 and η_0 are the temperature coefficient of efficiency and the generation efficiency of the solar cell at the standard test condition ($I_b = 1000\text{W/m}^2$, $T_0 = 25\,^\circ\text{C}$), respectively.

The electrical efficiency of the PV modules of the CPC-PVT collector, η_m, is expressed as [41].

$$\eta_m = \tau_g \beta_c \eta_c \tag{5}$$

where τ_g is the transmissivity of glass, β_c is the packing factor of CPC.

The useable electrical energy from the CPC-PVT collector, E_{sol}, is calculated as [27].

$$E_{sol} = A_{rm} I_b \eta_m \times 10^{-3} \tag{6}$$

where A_{rm} is the area of the receiver covered by the PV module and I_b is the direct beam solar irradiance, W/m^2.

The overall thermal energy $Q_{overall}$ is calculated by the collected thermal energy and by the thermal equivalent of the generated electrical energy, and expressed by:

$$Q_{overall} = Q_{sol,en} + \frac{E_{sol}}{\gamma} \tag{7}$$

The energy efficiency of the partially covered CPC-PVT collector (η_{PVT}) can be expressed as [38].

$$\eta_{PVT} = \frac{Q_{overall}}{A_a I_b} \tag{8}$$

where γ is electricity generation efficiency based on a natural gas plant, 0.38 [38]. A_a is total aperture area for CPC-PVT.

The exergy output of the partially covered CPC-PVT collector includes the electrical output and thermal energy, and its overall exergy efficiency, $\eta_{ex,PVT}$, is the sum of the exergy efficiency of the thermal energy and electrical efficiency of the PV module, and it is written as [42].

$$\eta_{ex,PVT} = \eta_m + \frac{Ex_{sol,ex}}{Ex_{sun,ex}} \tag{9}$$

The exergy of solar irradiance can be estimated as [43,44]:

$$Ex_{sun,ex} = I_b A_a \left[1 - \frac{4}{3}\frac{T_0}{T_{sun}} + \frac{1}{3}\frac{1}{f_f}\left(\frac{T_0}{T_{sun}}\right)^4\right] \times 10^{-3} \tag{10}$$

where $Ex_{sun,ex}$ is the exergy of solar irradiance, $Ex_{sol,ex}$ is the exergy of solar hot water, T_{sun} is the temperature of the sun, 6000 K [29]. f_f is the geometric factor ($f_f \geq \left(\frac{T_0}{T_{sun}}\right)^3$) [44].

3.2. ICE

The ICE model is taken from the literature [45], and some parameters including the electricity generation efficiency, outlet temperature of exhaust gas, and heat utilization efficiencies of exhaust gas and jacket water are obtained from the model (Table 2). The electricity generation efficiency is expressed as [46].

$$\eta_{ICE} = 0.2808 Ne^{0.0563} \tag{11}$$

where Ne is the nominal generation capacity of the ICE. The outlet temperature of the exhaust gas, T_{exh}, is calculated with the correlation of power capacity as [46]:

$$T_{exh} = 2 \times 10^{-5}(Ne)^2 - 0.0707 Ne + 758.33 \tag{12}$$

The heat utilization efficiencies of exhaust gas (η_{exh}) and jacket water (η_{jac}) can express as follows

$$\eta_{exh} = \frac{Q_{exh}}{Q_{ng}} \tag{13}$$

Table 2
ICE design parameters [45].

Natural gas	Major contains analysis, mol%	CH_4	C_2H_6	C_2H_4
		91.46	4.45	4
	Low heat value, MJ/Nm^3	37.96		
Nominal generation capacity, kW		100		
Excess air coefficient		1.12		
Heat utilization efficiency of exhaust gas, %		14.0		
Heat utilization efficiency of jacket water, %		31.0		

$$\eta_{jac} = \frac{Q_{jac}}{Q_{ng}} \tag{14}$$

where Q_{exh} and $Q_{jac}$are the waste heat of exhaust gas and jacket water, respectively. Q_{ng} is the inlet heat energy of natural gas.

3.3. The AHE

There are two forms of waste heat from the ICE: exhaust gas and jacket water. Due to their different properties, the two sources have different recovery potentials and economic effectiveness. Aiming to improve equipment utilization and simplify the energy flows, a utilization equipment is necessarily integrated to recover the waste heat from the two forms of heat sources. The mixed-effect LiBr-H_2O AHE driven by both the exhaust gas and hot water [47] is suitable to be applied, which flexibly recovers the waste heat with different ratios and has higher coefficient of performance (COP) than the single-effect absorption chiller. The direct-combustion of natural gas in the HG also supplements the heat deficiency. In this study, the three-source mixed-effect LiBr-H_2O AHE driven by the exhaust gas, mixed hot water, and natural gas is adopted to recover the waste heat, which is worked as an absorption chiller in summer and it can be worked as a heat exchanger in heating operating condition.

The AHE is modeled following [47]. The detailed assumptions and equations at the cooling operation condition can be found in the literature [48]. The mass balance, solute equilibrium, and energy balance equations for each AHE component are summarized as follows:

$$\sum m_{in} = \sum m_{out} \tag{15}$$

$$\sum m_{in} w_{in} = \sum m_{out} w_{out} \tag{16}$$

$$\sum m_{in} h_{in} = \sum m_{out} h_{out} \tag{17}$$

where m, w and h are mass, concentration and enthalpy of each stream, respectively.

3.4. The thermal energy storage (TES)

Ignoring the delay time during the heat storage and release, the volume of the TES tank, V_{TES}, can be estimated as [49]:

$$V_{TES} = \frac{Q_{TES}\eta_{TES}}{\rho_{TES} C_{TES}(T_{in} - T_{out})} \tag{18}$$

where Q_{TES} is the stored/released thermal energy into/from the TES tank. ρ_{TES} and C_{TES} are the density and specific heat of hot water, respectively. The heat transfer efficiency of the thermal storage tank, η_{TES}, is expressed to:

$$\eta_{TES} = \frac{Q_{TES}}{Q_{TES} + Q_{los}} \tag{19}$$

The heat loss, Q_{los}, can be expressed by the correlation [49]:

$$Q_{los} = K_{TES} F_{TES}(T_{TES} - T_a)\tau \tag{20}$$

where K_{TES} and F_{TES} are the average heat transfer coefficient and surface area of the TES tank, respectively. T_{TES} is the internal temperature of the water tank, and τ is the operation time. After obtaining the heat loss, the temperature in the TES tank can be estimated according to the energy balance.

4. Performance evaluation criteria

(1) Waste heat utilization efficiency of coupled system

The waste heat in this paper contains waste heat from the exhaust gas and jacket water, solar hot water, and auxiliary heat from natural gas used in heat shortage conditions. The waste heat utilization efficiency is defined as the ratio of the total energy outputs of cooling/heating and domestic hot water to the total waste heat, which is written as

$$\eta_{waste} = \begin{cases} \dfrac{Q_{cool} + Q_{dom}}{Q_{exh} + Q_{jac} + Q_{sol,en} + Q_{au}} & \text{(cooling)} \\ \dfrac{Q_{heat} + Q_{dom}}{Q_{exh} + Q_{jac} + Q_{sol,en} + Q_{au}} & \text{(heating)} \end{cases} \tag{21}$$

where $Q_{sol,en}$ and Q_{au} are the hot water from the CPC-PVT, and the auxiliary heat energy, respectively; Q_{cool}, Q_{heat}, and Q_{dom} are the cooling, heating, and domestic hot water outputs of the hybrid system, respectively.

(2) Energy and exergy efficiencies

The energy efficiency, η_{sys}, and the exergy efficiency, $\eta_{ex,sys}$, are employed to evaluate the coupled system's performances from the first and second thermodynamic laws, respectively, and they are expressed as

$$\eta_{sys} = \begin{cases} \dfrac{E_{out} + Q_{cool} + Q_{dom}}{Q_{sol} + Q_{ng}} & \text{(cooling)} \\ \dfrac{E_{out} + Q_{heat} + Q_{dom}}{Q_{sol} + Q_{ng}} & \text{(heating)} \end{cases} \tag{22}$$

$$\eta_{ex,sys} = \begin{cases} \dfrac{E_{out} + \left(\dfrac{T_0}{T_{ch}} - 1\right)Q_{cool} + \left(1 - \dfrac{T_0}{T_{dom}}\right)Q_{dom}}{Ex_{sol} + Ex_{ng}} & \text{(cooling)} \\ \dfrac{E_{out} + \left(1 - \dfrac{T_0}{T_{heat}}\right)Q_{heat} + \left(1 - \dfrac{T_0}{T_{dom}}\right)Q_{dom}}{Ex_{sol} + Ex_{ng}} & \text{(heating)} \end{cases} \tag{23}$$

where E_{out} is the electricity output of the hybrid system; Q_{sol} is the inlet solar energy; Ex_{sol} and Ex_{ng} are the inlet exergy energy of solar and natural gas, respectively; T_{cool}, T_{dom}, and T_{heat} are the average temperatures of chilled water, domestic hot water, and space heating water, respectively. T_0 is the reference temperature; to evaluate the performance, the reference temperature is set as 298.15 K.

(3) Primary energy saving ratio (PESR) and CO_2 emission reduction ratio (CDERR)

To compare between the hybrid CCHP system and the conventional CCHP system without solar energy, the primary energy saving ratio (PESR) and carbon dioxide emission reduction ratio (CDERR) are employed to evaluate the benefits achieved by the hybrid system, and they are expressed respectively as

$$PESR = \frac{Q_{ref} - Q_{sys}}{Q_{ref}} \tag{24}$$

$$CDERR = \frac{CDE_{ref} - CDE_{sys}}{CDE_{ref}} \tag{25}$$

where Q_{ref} and Q_{sys} are the energy consumption of the reference CCHP system and the hybrid system, respectively; CDE_{ref} and CDE_{sys} are the carbon dioxide emissions of the reference CCHP system and the hybrid system, respectively. Owing to their different contributions of solar energy and natural gas, the direct adding of primary energy sources could weaken the contribution of solar energy [48]. Consequently, according to the principle in the literature [50] for multi-energy thermal complementary systems, the equivalent energy consumption of the hybrid is defined as

$$Q_{sys} = Q_{ng} + Q_{sol}\eta_{cc} + Q_{sol}\frac{\eta_m}{\eta_{ng}} \tag{26}$$

where η_{cc} is the thermal efficiency of the Carnot cycle ($\eta_{cc} = 1 - \frac{T_0}{T_{sol}}$), T_{sol} is the collection temperature, and η_{ng} is the electricity generation efficiency of natural-gas-fired power plant. The solar energy through the CPC-PVT is converted into heat and electricity, the heat energy based on the collection temperature transfers to the equivalent energy consumption of traditional fossil energy, and similarly, the electricity from the CPC-PVT is converted to the equivalent energy according to the electricity generation efficiency of a natural-gas-fired power plant.

5. Results and discussion

5.1. Validation of models

There are four main components including ICE, CPC-PVT, AHE and TES in the simulation by the Engineering Equation Solver (EES) software [51]. These models were validated by the following methods:

(1) The ICE model, especially the electricity generation efficiency and the outlet temperature of exhaust gas was fitted by using the data from a series of engines of the AB group from Ref. [46].
(2) The AHE model has been validated in the literature [48] through comparing to the results from Ref. [47]. The relative errors of average enthalpy, concentration, pressure and temperature of 14 states were <1%. Although the relative error of mass flow was somewhat larger, 12.71%, but considering its small magnitude, which varies from 0.0034 to 0.248 kg/s, it is acceptable. Moreover, the COP variations of AHE with the proportions of hot water to exhaust gas are computed and also compared to Ref. [47], and the root-mean-square error is approximately 5.4%.
(3) Ignoring the transient conditions, the TES tank is operated as a heat exchanger, and the heat transfer efficiency of heat exchanger was set to 0.9 as in Ref. [9].
(4) As the CPC-PVT subsystem, the heat transfer coefficient and solar cell temperature are the essential parameters that influence the solar hot water and electricity. To validate the modeling, the comparisons of the heat transfer factors between the simulation results and the data from Ref. [37] are summarized in Table 3. The average relative error is 0.17%, testifying to the accuracy of the heat transfer model of this CPC-PVT. In addition, the comparisons of solar cell

Table 3
Comparisons of heat transfer factors (their definitions are included in the Nomenclature).

Parameter	Value (W/m^2 K)	Ref [37]	Parameter	Value	Ref [37]
U_{L1}	3.47	3.47	PF_1	0.3782	0.3782
$U_{L,m}$	7.88	7.87	PF_2	0.9517	0.9512
$U_{tc,a}$	9.18	9.17	PF_c	0.9482	0.9842
U_{Lc}	4.73	4.70			
$U_{tc,p}$	5.58	5.58			
$U_{tp,a}$	4.81	4.80			

temperature at the same ambient parameters and the mass flow with 0.012 kg/s [37] are shown in Fig. 3. The root-mean-square error is approximately 6.6%, which is acceptable.

5.2. Case study

A three-floor hotel building in Beijing with 500 m^2 roof area was selected as the case study. The average main celling height is 3.6 m, and the total area of the windows and glazing comprises about 30% of the total wall area. The hourly cooling and heating loads were simulated in the DesT Software [52] based on the similar building model in Ref. [53], and the hourly electric loads were obtained according to the operation strategy of lights and equipment in the DesT simulation model [53]. The simulation has default DesT values by hotel building for building shell, structure, materials and shades and the parameters of heating, ventilating and air conditioning system have default DesT values such as fresh air per person, heat emission of human body and the temperature and humidity setting points.

The hourly loads are displayed in Fig. 4, and the maximal loads of electricity, cooling, and heating were found to be 100 kW, 140 kW, and 159 kW, respectively. The capacities of the CCHP system are determined by these maximal loads. The available roof area for the CPC-PVT installation is approximately 328 m^2.

Table 4 lists the base design parameters. Aiming to approach the temperature of jacket water at state 9 in Figs. 1 and 85 °C, the temperature of the water at state 11 from the CPC-PVT is determined according to collector installation area and solar irradiance. When the solar irradiance is set to 800 W/m^2 in summer cooling operation mode [48], two series-connected CPC-PVT collectors described in Table 1 (the total area of each collector aperture is about 2 m^2) are used, and the outlet temperature will reach 85.3 °C. The solar collection system consists of 82 sets of collectors installed in parallel on the fixed roof area. In winter, the solar irradiance is assumed to be 700 W/m^2 and the outlet temperature of two collectors in series is 80.9 °C.

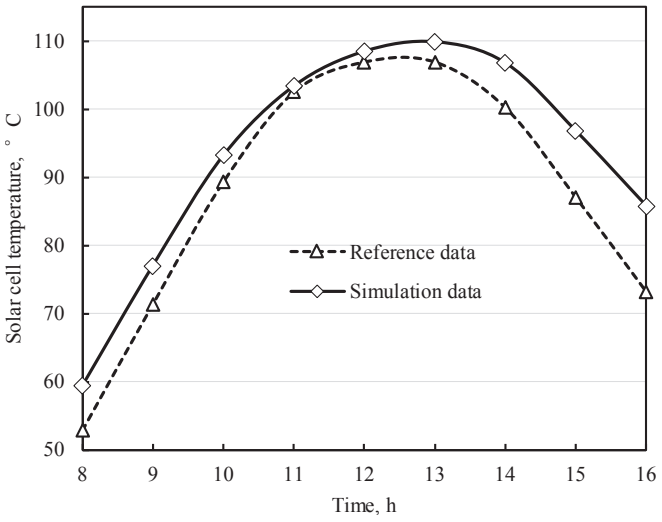

Fig. 3. Comparisons of solar cell temperature between simulation and literature data.

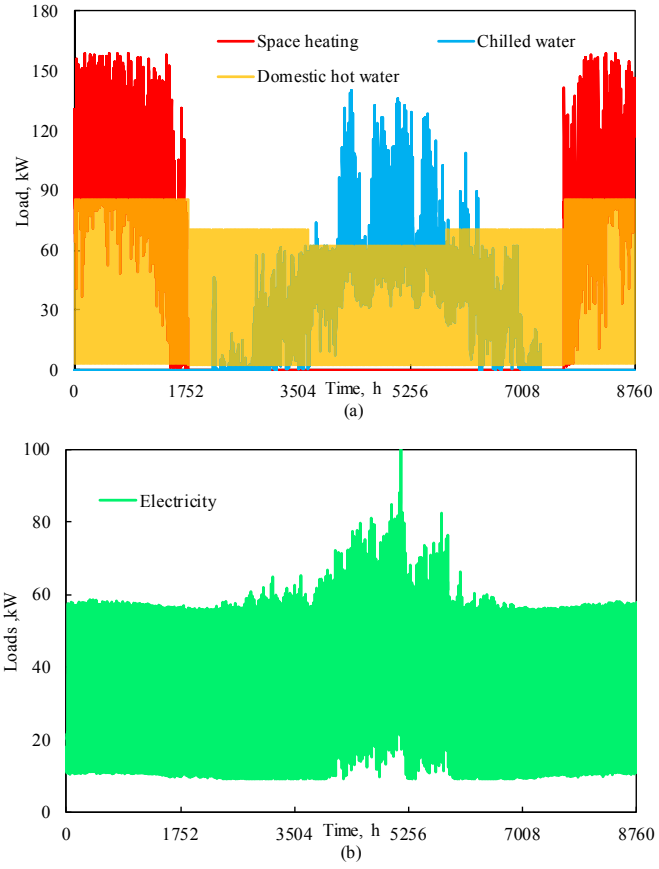

Fig. 4. Hourly demands of the hotel building.

5.3. Performance at the design operating conditions

Fig. 5 displays the simulation procedure of the hybrid CCHP system using the EES software, and its thermodynamic performances in design condition are listed in Table 5. The total solar energy inputs of the CPC-PVT are 231 kW and 202 kW, respectively, where the solar irradiance was assumed to be 800 W/m^2 in summer and 700 W/m^2 in winter. Combined to the ICE, the maximal electricity outputs of the coupled system are 108 kW in the cooling mode, and 107 kW in the heating mode. The space cooling and heating outputs are 195 kW and 167 kW, respectively. Half of the steam generated by the high-pressure generator (state b8 in Fig. 1) is used to produce the domestic hot water, 16 kW output in summer, and 19 kW in winter. Regarding the coupled system, its waste heat utilization efficiency in the cooling condition, 92.5%, is just slightly higher than that in the heating condition, 91.9%.

For the CPC-PVT subsystem, its energy efficiency is 83.6% in summer and 74.6% in winter, while the exergy efficiency in summer, 19.8%, is lower than that in winter, 24.7%. These can be explained by the increasing generation efficiency of the PV module in winter, while the thermal energy output decreases owing to the lower ambient temperature and larger overall heat losses. Analyzing the exergy destruction in summer, the CPC-PVT and ICE account for 54.8% and 38.2% of total exergy destruction and loss of

Table 4
Base design parameters of hybrid CCHP system.

Component	Parameter	Value	Ref
Building loads	Electricity, kW	100	
	Cooling, kW	140	
	Heating, kW	159	
CPC-PVT	Single collector aperture, m^2	2	[54]
	Concentration ratio	2	[25]
	Mass flow, kg/s	0.02	
	Pieces of collectors	164	
	Total aperture area of collectors, m^2	328	
ICE	Jacket water temperature, °C	85/70 (states 9/20)	[45]
	Exhausted gas temperature, °C	470/170/120 (states 6/7/8)	[45]
AHE	Absorber temperature, °C	38	[22]
	Cooling water temperature, °C	32/36 (states a7/a8)	[22]
	Evaporation temperature, °C	5	[22]
	Condensing temperature, °C	83	[22]
	Chilled water temperature, °C	7/14 (states a5/a6)	[22]
	Space heating water temperature, °C	55/65 (states a3/a4)	
	Domestic hot water temperature, °C	60 (state a10)	
TES	Space heating water temperature, °C	55/65 (states a11/a12)	
	Domestic hot water temperature, °C	60 (state a2)	

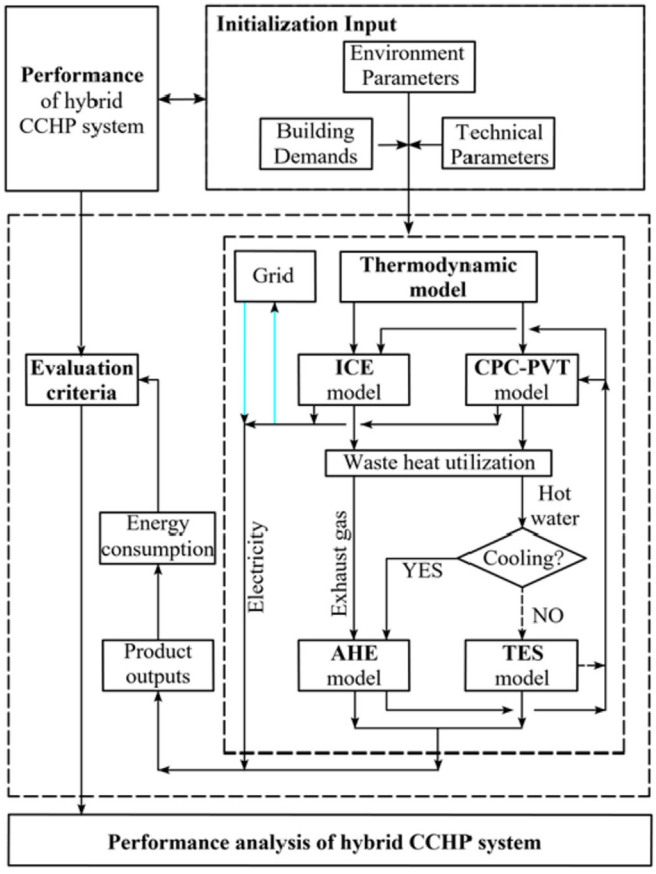

Fig. 5. Computational procedures of hybrid system.

the hybrid system respectively. Due to the larger contributions of the AHE and CPC-PVT in the cooling work condition, the overall energy efficiency of the hybrid system in summer, 63.3%, is larger than that in winter, 61.7%. The overall exergy efficiency in summer is, however, lower than that in winter because the exergy of the chilled water is much lower than that of the hot water.

Compared to the CCHP system without solar energy in Ref. [22], the energy efficiency of the hybrid system integrated with CPC-PVT becomes low because the utilization efficiency of solar energy is less than natural gas. However, compared to the hybrid system integrated with solar heat collectors and PV panels separately in Ref. [55], both the energy and exergy efficiencies in this study are larger than the efficiencies (the energy and exergy efficiencies in the cooling mode are 46.8% and 20.9%, respectively, and they in the heating mode are 53.7% and 24.9%, respectively.) in Ref. [55] at the same solar area, which demonstrates that the CPC-PVT is an effective integration to improve efficiency and reduce installation area.

Table 5
Simulation results on the design operating conditions.

Items	Parameters	Summer	Winter
System inputs	Natural gas, kW	273	273
	Solar irradiance, W/m^2	800	700
	Solar energy, kW	231	202
System outputs	Electricity, kW	108	107
	Space cooling/heating, kW	195	167
	Domestic hot water, kW	16	19
Performances	Waste heat utilization efficiency, %	92.5	91.9
	Energy efficiency of CPC-PVT, %	83.4	76.5
	Exergy efficiency of CPC-PVT, %	19.8	24.7
	Energy efficiency of hybrid CCHP, %	63.3	61.8
	Exergy efficiency of hybrid CCHP, %	21.8	27.1

5.4. Performances at off-design operating conditions

The direct beam solar irradiance (I_b) and power generation of the ICE vary with the weather and building demands in the actual operation, which are the key parameters influencing the system performances. In the following section, the energy and exergy efficiencies of subsystems are analyzed under variable environmental conditions.

5.4.1. Performance of CPC-PVT subsystem

Fig. 6 displays the variations of energy and exergy efficiencies, and the total output of the CPC-PVT with solar irradiance. The simulation of CPC-PVT indicated that no solar hot water is output from the CPC-PVT when the I_b is lower than 212 W/m^2 in summer or 286 W/m^2 in winter, because the outlet temperature is lower than the temperature of the jacket water, 70 °C. Because the generation efficiency of the PV module becomes linearly with the down toward owing to the increasing solar cell temperature, both the energy and exergy efficiencies increase while the I_b decreases

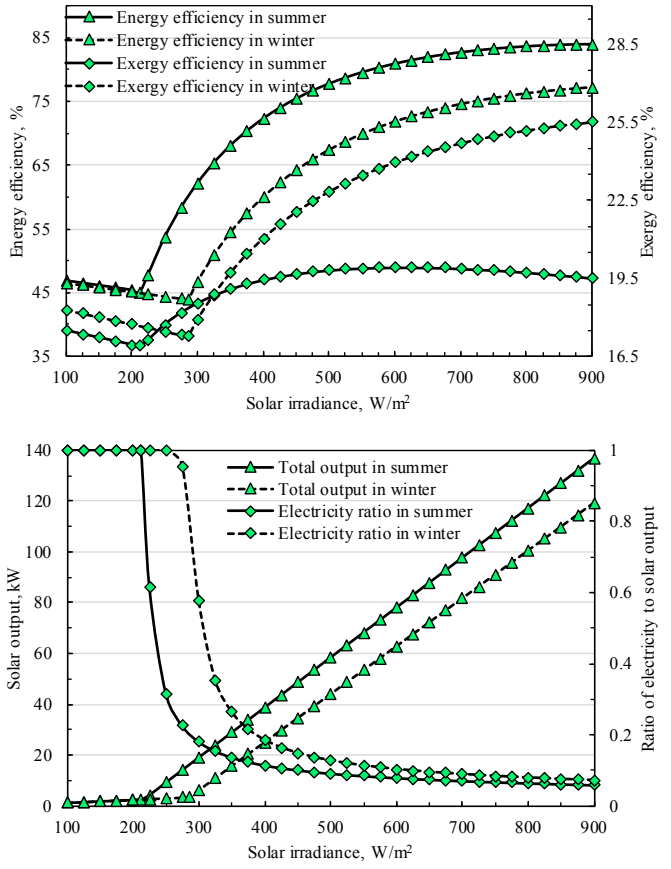

Fig. 6. The energy and exergy efficiencies of CPC-PVT subsystem as function of the solar irradiance (I_b).

below the critical point. The minimal solar energy and exergy efficiencies of the CPC-PVT subsystem in summer are 45.3% and 16.9%, respectively, while they are 46.3% and 17.3% in winter, as shown in Fig. 6(a). This difference is primarily because the ambient temperature in winter is lower than that in summer.

When the I_b is larger than the critical value, the energy efficiency increases with increasing I_b, but at a decreasing rate. The energy efficiency under the cooling operating condition (Fig. 6(a)) is always higher than that under the heating work condition, thus resulting in higher outputs in summer, as shown in Fig. 6(b). Although the hybrid system exhibits a higher energy efficiency in summer, its exergy efficiency in summer is not always larger than that in winter. Even at the higher I_b, the exergy efficiency in summer is lower because the ratio of electricity to solar output from the CPC-PVT collector becomes lower with increasing I_b, as shown in Fig. 6(b). The exergy of per unit of electricity energy is larger than that of the solar hot water.

The curve showing the dependence of the exergy efficiency in summer is unlike the other three curves. When the I_b exceeds the critical point, the exergy efficiency increases at a high rate until it reaches its maximal value, 20.0%, at the solar irradiance of 600 W/m^2. It decreases slightly with the increase of the I_b. These results in changes in the ratio of electricity to solar output from the CPC-PVT. It clearly demonstrates that this ratio becomes lower with increasing I_b in Fig. 6(b). Both the increasing outputs and decreasing ratio of electricity to solar output influence the changes in exergy efficiency. Unlike the changes in exergy efficiency of CPC-PVT in summer, the exergy efficiency during the studied ranges on the heating work condition always increases with increasing I_b after the critical point of 286 W/m^2. With the increase of I_b, the temperatures of the PV and absorber plates have a negative influence on the solar electricity output, while they have a positive influence in the solar thermal output in summer. The impact is lower in winter because higher thermal losses occur from the subsystem to the ambient.

5.4.2. Waste heat utilization performance of the hybrid system

The performance of the waste heat utilization system is related to the fractional contribution of the input energy sources, especially the ICE and CPC-PVT. The load factor of the ICE which is defined as the ratio of actual electricity output from ICE to nominal capacity and the solar irradiance are selected here to discuss their impacts on the waste heat utilization efficiency.

Fig. 7 displays the variations of the waste heat utilization efficiency of the hybrid system with the ICE load ratio and solar irradiance at the two operating conditions. Four boundaries and four endpoints exist in each waste heat utilization efficiency surface, such as curves L1, L2, L3, and L4, and endpoints P1, P2, P3, and P4 in Fig. 7(a). Each boundary curve denotes the waste heat utilization

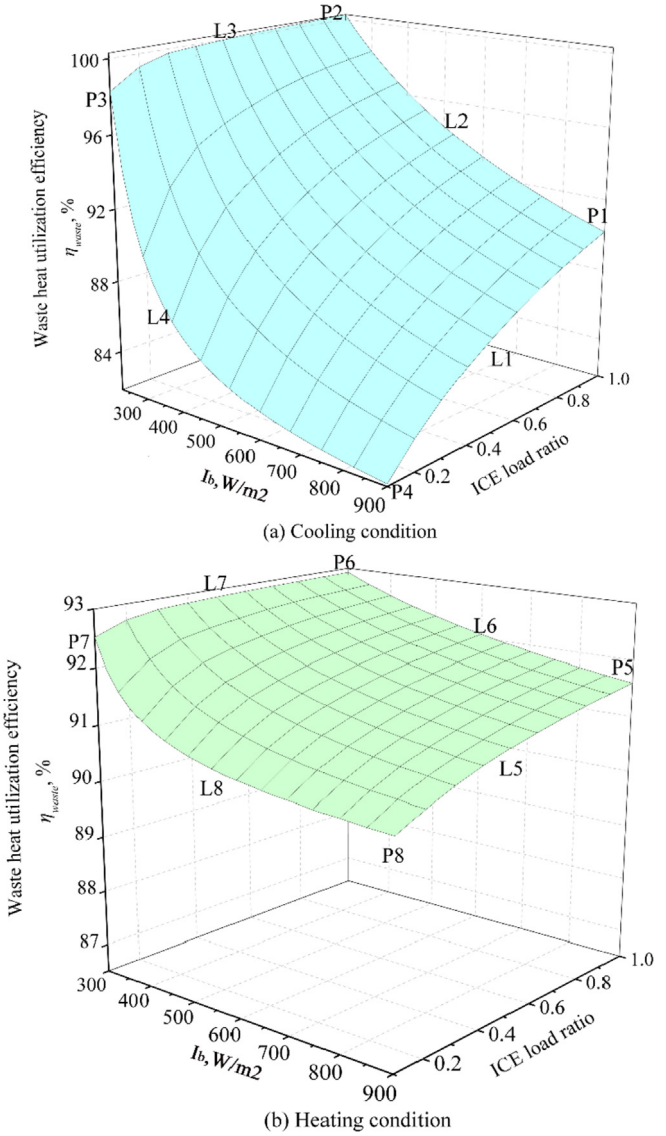

Fig. 7. Variations of waste heat utilization efficiency (η_{waste}) with the ICE load ratio and solar irradiance (I_b) on the cooling and heating work conditions.

efficiency variation with one of the parameters, while another parameter is maintained constant, as the lowest or the largest. For example, the η_{waste} on the cooling work condition increases with the increasing ICE load ratio, as shown in the curve L3 when the I_b is maintained as the lowest value, 225 W/m^2; subsequently, the η_{waste} reaches the maximum value, 100.3%, as endpoint P2. Contrarily, the η_{waste} decreases with increasing I_b, as shown by the curves L4 and L2, which resulted from the higher ratio of heat input of the low-pressure generator to that of the high-pressure generator. The increasing I_b always causes the hot water to increase while the exhaust gas doesn't change at the fixed ICE load ratio. Subsequently, point P1 indicates that the hybrid system is operated under the full load of the ICE while the I_b is 900 W/m^2, and the η_{waste} is 90.2%.

Comparing Fig. 7(a) and (b), we found that the influence of two variable parameters on the η_{waste} on the heating work condition is similar to those on the cooling work condition. However, the hybrid system exhibits a stable performance, in which the η_{waste} varies from 90.3% to 92.9%. This indicates that the hybrid system has a complementary design and different operation flow in winter: the TES and AHE subsystems are operated as heat exchangers in winter conditions. Additionally, when the ICE is operated with a constant load, 0.1, the η_{waste} decreases slowly from 92.5% (as shown in point P7), to 90.3% (as shown in point P8). Thus, compared to the η_{waste} in summer, an increasing I_b has a lower impact in the heating work condition.

5.4.3. Thermodynamic performance of the hybrid system

The variations of energy efficiency for the different working conditions are shown in Fig. 8. Fig. 8(a) indicates that the increases in I_b and ICE load ratio yield opposite effects on the energy efficiency for the cooling work condition. The ICE load ratio has a positive influence on the η_{sys} (energy efficiency) while the higher I_b causes it to operate less slowly. The primary reason is that the contribution of solar energy from the CPC-PVT to the η_{sys} is less than the ICE, although the higher I_b improves the η_{sys} of the CPC-PVT. In addition, as shown in the analysis in Fig. 7(a), the η_{waste} decreases with increasing I_b owing to the higher ratio of the heat input of the low-pressure generator to that of the high-pressure generator. Consequently, the higher the I_b is, the lower the η_{sys} of the input energy resources is.

Contrary to the negative influence of the solar energy magnitude on the η_{sys} in summer shown in Fig. 8(a), the η_{sys} on the heating work condition increases steeply with increasing I_b at the lower ICE load ratio shown as curve L8, while the increasing rate will become lower at the higher ICE load ratio shown as curve L6. The η_{sys} is related to the outputs of the products and inputs of solar energy and natural gas. At the fixed ICE load ratio (e.g., curve L8), the natural gas input and waste heat from the ICE are maintained constant. Further, an increased I_b corresponds to an increased solar energy input that affects solar outputs positively. Moreover, the thermal efficiency of the CPC-PVT subsystem demonstrates a same trend with the increasing I_b. Thus, the solar thermal energy, which directly influences the domestic hot water and heating outputs, has a higher increasing rate than the solar inputs; further, the η_{waste} has a more stable performance than that in summer; it varied within a smaller range, from 92.5% to 90.3%, as shown by the curve L8 in Fig. 7(b).

Then analyzing the adjustment ranges of the cooling (heating) to electricity ratio, which is defined as the total cooling (heating) output to the total electricity in Fig. 8, it is observed that the highest ratios in the cooling and heating modes are 6.14 (point P4) in Figs. 8 (a) and 6.00 (point P8) in Fig. 8 (b), respectively. Compared to the CCHP system without solar energy (1.35) and the system assisted by TES (2.24) in Ref. [22], the adjustment ranges of the hybrid system are much wider, which demonstrated that the hybrid CCHP system has a more flexible ability to meet the dynamic and variable loads.

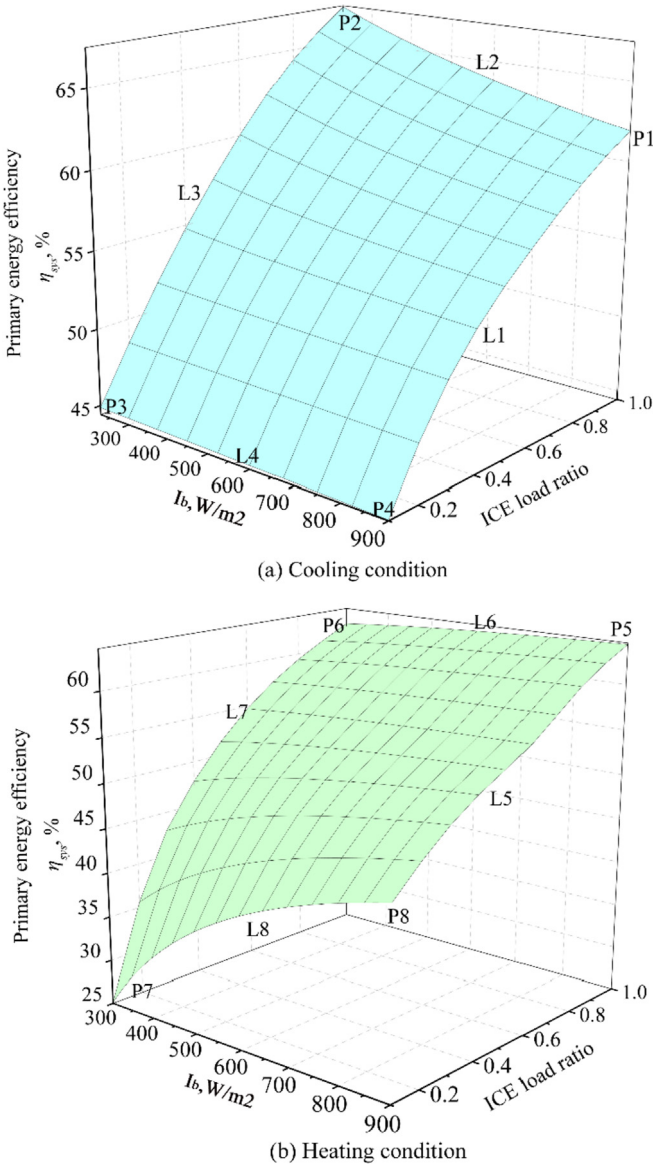

Fig. 8. Variations of energy efficiency (η_{sys}) with the ICE load ratio and solar irradiance (I_b). on the cooling and heating work conditions.

Fig. 9 displays the exergy efficiency variations of the cooling and heating work conditions. The $\eta_{ex,sys}$ (exergy efficiency) rises with the ICE load ratio at fixed I_b, as shown by the curves L1 and L3 in Fig. 9(a). The $\eta_{ex,sys}$ improves from 7.6% (point P4) to 20.6% (point P1), and from 12.9% (point P3) to 29.5% (point P2), when the ICE load ratio is increased from 0.1 to 1.0. The I_b, however, affects the $\eta_{ex,sys}$ negatively. This is primarily because the electrical efficiency of the PV module decreases linearly with increasing PV temperature caused by increasing I_b. The $\eta_{ex,sys}$ of the PV module decreases significantly although the solar electricity improves as the I_b increases.

In winter, as shown in Fig. 9(b), the variations of $\eta_{ex,sys}$ are similar to those in summer. The $\eta_{ex,sys}$ improves from 12.2% (point P8) to 25.5% (point P5), and from 12.9% (point P7) to 31.9% (point P6) with increasing ICE load ratio, as the curves L5 and L7, respectively, when the I_b is 300 W/m^2 and 900 W/m^2, respectively. The primary reason for these phenomena is that the electricity produced by ICE and the CPC-PVT subsystem has a higher exergy

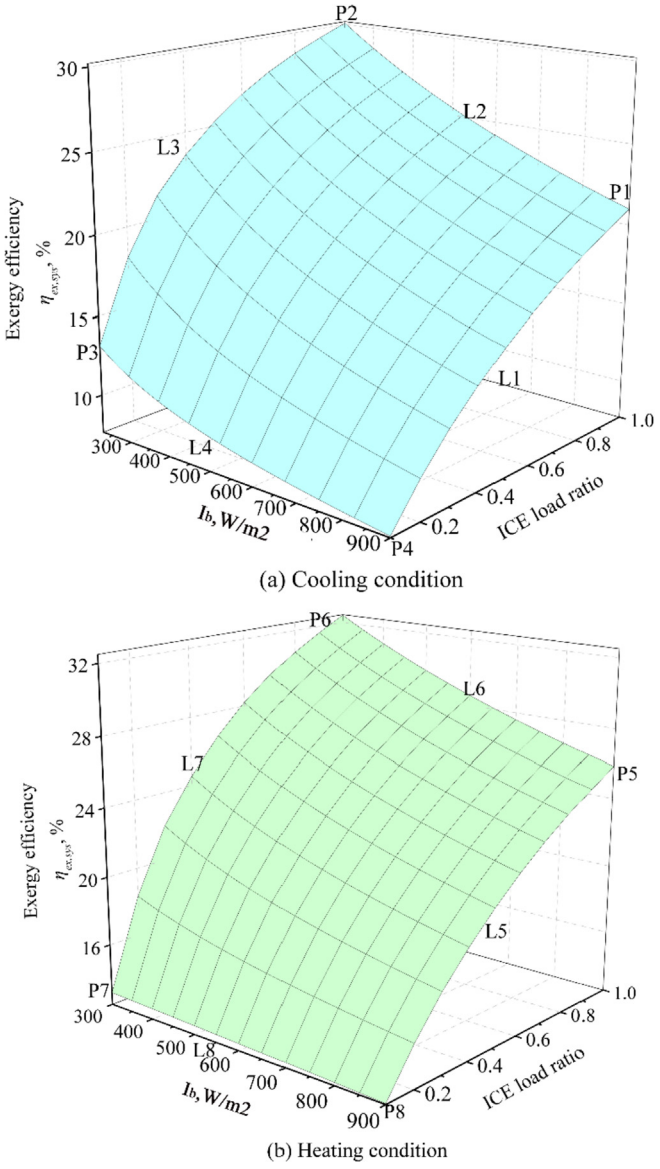

Fig. 9. Variations of exergy efficiency ($\eta_{ex,sys}$) with the ICE load ratio and solar irradiance (I_b) on the cooling and heating work conditions.

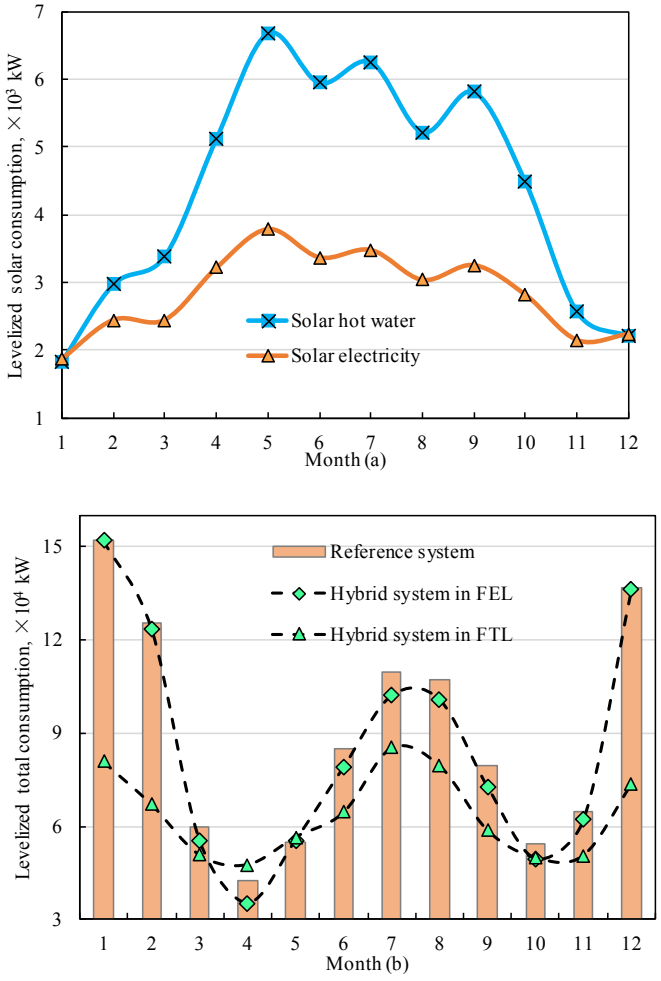

Fig. 10. Energy consumptions of the hybrid system and reference system.

than the solar hot water and recovered heat from the ICE at the same energy. When the I_b increases, the generation efficiency declines significantly due to the increased solar cell temperature, as shown in Eq. (3). Additionally, an increase in the ICE load ratio leads to an increasing electricity generation efficiency, as shown in Eq. (11).

5.5. Energy and environmental benefits achieved by the hybrid system

In order to analyze the energy and environment benefits of the hybrid system, a conventional CCHP system without solar energy in Ref. [22] is used as a reference. The reference system which consists of ICE, AHE, and TES subsystems operates with following electrical load (FEL) mode. The hot water tank is used to store the excess heat or supplement the heat while the heat shortage occurs.

Fig. 10 displays the energy consumptions of the hybrid CCHP system in FEL and following thermal load (FTL) operating modes and the reference CCHP system. The monthly levelized energy consumption of solar energy is shown in Fig. 10(a). For the whole year, the levelized consumption caused by solar hot water is larger than the levelized solar electricity consumption. Moreover, in summer, both the solar water and electricity consumption is higher than the consumption in other conditions. This can be concluded that the hybrid system gets the higher solar input in summer due to the higher beam solar irradiance.

Fig. 10(b) shows the levelized total energy consumption of two systems. It can be observed that the reference CCHP system consumes the largest natural gas while the hybrid system in FTL mode consumes the least energy. The levelized PESR of the hybrid system in the FTL mode is 28.6%, and the CDERR is 36.7% due to the decrease of natural gas consumption. When the system operates in FEL mode, the PESR and CDERR of the hybrid system are 4.6% and 12.7% respectively.

6. Conclusions

This paper proposed a novel hybrid CCHP system integrated with CPC-PVT solar collectors, presented the thermodynamic analysis on the design and off-design operating conditions, and obtained the energy and environmental benefits achieved by the hybrid system. The following conclusions were obtained:

The integration of CPC-PVT collectors was found to be an effective method to match and supplement the electricity and heat outputs of the natural gas CCHP system. Regarding the specific

design parameters, the energy efficiencies of the hybrid system in the cooling and heating modes reach 63.3% and 61.8%, respectively, and their exergy efficiencies are 21.8% and 27.1%, respectively. Compared to the separate installations of solar heat collector and PV panels in natural gas CCHP system, the hybrid CCHP system integrated with CPC-PVT improves at least energy efficiency by 8.1% and exergy efficiency by 0.9%.

The off-design analysis demonstrates that the increasing solar irradiance leads to the decrease of energy and exergy efficiencies on the cooling work condition and the exergy efficiency on the heating work condition, because the solar energy utilization efficiency is less than the natural gas. However, it has a positive impact on the energy efficiency on the heating work condition which results from the different energy flowcharts of mixed hot water. Compared to the natural gas CCHP system without solar energy, the hybrid system has more flexible ability to adjust the ratio of cooling (heating) to electricity to satisfy the dynamic loads of users.

Evaluations using only energy and exergy efficiencies to demonstrate the thermodynamic performances of the hybrid CCHP system could not identify the mechanism for improving its performance, and the levelized PESR and CDERR were found to be more suitable for demonstrating the contributions of solar energy. Compared to the CCHP system without solar energy, the maximum levelized PESR achieved by the hybrid system in FTL mode is 28.6%, and the maximum CDERR is 36.7%. It indicates that the proposed hybrid system offers significant benefits over the conventional natural-gas-fired CCHP system.

Declaration of interests

☒ The authors declare that they have no known competing financial interests or personal relationships that could have appeared to influence the work reported in this paper.

☐ The authors declare the following financial interests/personal relationships which may be considered as potential competing interests.

Acknowledgements

This research has been supported by National Natural Science Foundation of China (Grant No. 51876064 to co-authors Wang, Chen, and Li).

References

[1] Cho H, Smith AD, Mago P. Combined cooling, heating and power: a review of performance improvement and optimization. Appl Energy 2014;136:168–85.
[2] Wu DW, Wang RZ. Combined cooling, heating and power: a review. Prog Energy Combust Sci 2006;32(5):459–95.
[3] Mancarella P. MES (multi-energy systems): an overview of concepts and evaluation models. Energy 2014;65:1–17.
[4] Hassan HZ, Mohamad AA. Thermodynamic analysis and theoretical study of a continuous operation solar-powered adsorption refrigeration system. Energy 2013;61:167–78.
[5] Ju L, Tan Z, Li H, Tan Q, Yu X, Song X. Multi-objective operation optimization and evaluation model for CCHP and renewable energy based hybrid energy system driven by distributed energy resources in China. Energy 2016;111:322–40.
[6] Wang J, Mao T, Wu J. Modified exergoeconomic modeling and analysis of combined cooling heating and power system integrated with biomass-steam gasification. Energy 2017;139:871–82.
[7] Wang J, Li M, Ren F, Li X, Liu B. Modified exergoeconomic analysis method based on energy level with reliability consideration: cost allocations in a biomass trigeneration system. Renew Energy 2018;123:104–16.
[8] Toro C, Lior N. Analysis and comparison of solar-heat driven Stirling, Brayton and Rankine cycles for space power generation. Energy 2017;120:549–64.
[9] Wang J, Lu Z, Li M, Lior N, Li W. Energy, exergy, exergoeconomic and environmental (4E) analysis of a distributed generation solar-assisted CCHP (combined cooling, heating and power) gas turbine system. Energy 2019;175:1246–58.
[10] Yue T, Lior N. Thermodynamic analysis of solar-assisted hybrid power generation systems integrated with thermochemical fuel conversion. Energy 2017;118:671–83.
[11] Yue T, Lior N. Thermal hybrid power systems using multiple heat sources of different temperature: thermodynamic analysis for Brayton cycles. Energy 2018;165:639–65.
[12] Khaliq A, Kumar R, Mokheimer EMA. Investigation on a solar thermal power and ejector-absorption refrigeration system based on first and second law analyses. Energy 2018;164:1030–43.
[13] Ondeck AD, Edgar TF, Baldea M. Impact of rooftop photovoltaics and centralized energy storage on the design and operation of a residential CHP system. Appl Energy 2018;222:280–99.
[14] Yu D, Zhu H, Han W, Holburn D. Dynamic multi agent-based management and load frequency control of PV/Fuel cell/wind turbine/CHP in autonomous microgrid system. Energy 2019;173:554–68.
[15] Zhang N, Wang Z, Lior N, Han W. Advancement of distributed energy methods by a novel high efficiency solar-assisted combined cooling, heating and power system. Appl Energy 2018;219:179–86.
[16] Yang G, Zhai X. Optimization and performance analysis of solar hybrid CCHP systems under different operation strategies. Appl Therm Eng 2018;133:327–40.
[17] Ni J, Zhao L, Zhang Z, Zhang Y, Zhang J, Deng S, et al. Dynamic performance investigation of organic Rankine cycle driven by solar energy under cloudy condition. Energy 2018;147:122–41.
[18] Li X, Shen Y, Kan X, Hardiman TK, Dai Y, Wang C-H. Thermodynamic assessment of a solar/autothermal hybrid gasification CCHP system with an indirectly radiative reactor. Energy 2018;142:201–14.
[19] Su B, Han W, Chen Y, Wang Z, Qu W, Jin H. Performance optimization of a solar assisted CCHP based on biogas reforming. Energy Convers Manag 2018;171:604–17.
[20] Buonomano A, Calise F, Ferruzzi G, Vanoli L. A novel renewable polygeneration system for hospital buildings: design, simulation and thermo-economic optimization. Appl Therm Eng 2014;67(1):43–60.
[21] Calise F, Dentice d'Accadia M, Palombo A, Vanoli L. Dynamic simulation of a novel high-temperature solar trigeneration system based on concentrating photovoltaic/thermal collectors. Energy 2013;61:72–86.
[22] Wang J, Xie X, Lu Y, Liu B, Li X. Thermodynamic performance analysis and comparison of a combined cooling heating and power system integrated with two types of thermal energy storage. Appl Energy 2018;219:114–22.
[23] Tiwari S, Agrawal S, Tiwari GN. PVT air collector integrated greenhouse dryers. Renew Sustain Energy Rev 2018;90:142–59.
[24] Aste N, Del Pero C, Leonforte F. Water PVT collectors performance comparison. Energy Procedia 2017;105:961–6.
[25] Tripathi R, Tiwari GN, Bhatti TS, Dwivedi VK. 2-E (Energy-Exergy) for partially covered concentrated photovoltaic thermal (PVT) collector. Energy Procedia 2017;142:616–23.
[26] Proell M, Osgyan P, Karrer H, Brabec CJ. Experimental efficiency of a low concentrating CPC PVT flat plate collector. Sol Energy 2017;147:463–9.
[27] Elsafi AM, Gandhidasan P. Comparative study of double-pass flat and compound parabolic concentrated photovoltaic–thermal systems with and without fins. Energy Convers Manag 2015;98:59–68.
[28] Zhang H, Liang K, Chen H, Gao D, Guo X. Thermal and electrical performance of low-concentrating PV/T and flat-plate PV/T systems: a comparative study. Energy 2019;177:66–76.
[29] Atheaya D, Tiwari A, Tiwari GN, Al-Helal IM. Analytical characteristic equation for partially covered photovoltaic thermal (PVT) compound parabolic concentrator (CPC). Sol Energy 2015;111:176–85.
[30] Tiwari GN, Meraj M, Khan ME, Mishra RK, Garg V. Improved Hottel-Whillier-Bliss equation for N-photovoltaic thermal-compound parabolic concentrator (N-PVT-CPC) collector. Sol Energy 2018;166:203–12.
[31] Chen Y, Wang J, Ma C, Gao Y. Thermo-ecological cost assessment and optimization for a hybrid combined cooling, heating and power system coupled with compound parabolic concentrated-photovoltaic thermal solar collectors. Energy 2019;176:479–92.
[32] Saini V, Tripathi R, Tiwari G, Al-Helal M. Electrical and thermal energy assessment of series connected N partially covered photovoltaic thermal (PVT)-compound parabolic concentrator (CPC) collector for different solar cell materials. Appl Therm Eng 2018;128:1611–23.
[33] Kasaeian A, Nouri G, Ranjbaran P, Wen D. Solar collectors and photovoltaics as combined heat and power systems: a critical review. Energy Convers Manag 2018;156:688–705.
[34] Tiwari GN, Meraj M, Khan ME. Exergy analysis of N-photovoltaic thermal-compound parabolic concentrator (N-PVT-CPC) collector for constant collection temperature for vapor absorption refrigeration (VAR) system. Sol Energy 2018;173:1032–42.
[35] Mittelman G, Kribus A, Mouchtar O, Dayan A. Water desalination with concentrating photovoltaic/thermal (CPVT) systems. Sol Energy 2009;83(8):1322–34.
[36] Singh DB, Tiwari GN. Performance analysis of basin type solar stills integrated with N identical photovoltaic thermal (PVT) compound parabolic concentrator (CPC) collectors: a comparative study. Sol Energy 2017;142:144–58.
[37] Tripathi R, Tiwari GN, Al-Helal IM. Thermal modelling of N partially covered photovoltaic thermal (PVT) – compound parabolic concentrator (CPC) collectors connected in series. Sol Energy 2016;123:174–84.
[38] Tripathi R, Tiwari GN. Annual performance evaluation (energy and exergy) of fully covered concentrated photovoltaic thermal (PVT) water collector: an

experimental validation. Sol Energy 2017;146:180–90.
[39] Usón S, Uche J, Martínez A, del Amo A, Acevedo L, Á Bayod. Exergy assessment and exergy cost analysis of a renewable-based and hybrid trigeneration scheme for domestic water and energy supply. Energy 2019;168:662–83.
[40] Evans DL. Simplified method for predicting photovoltaic array output. Sol Energy 1981;27(6):555–60.
[41] Tiwari GN, Mishra RK, Solanki SC. Photovoltaic modules and their applications: a review on thermal modelling. Appl Energy 2011;88(7):2287–304.
[42] Sahota L, Tiwari GN. Review on series connected photovoltaic thermal (PVT) systems: analytical and experimental studies. Sol Energy 2017;150:96–127.
[43] Badescu V. How much work can be extracted from diluted solar radiation? Sol Energy 2018;170:1095–100.
[44] Kalogirou SA, Karellas S, Badescu V, Braimakis K. Exergy analysis on solar thermal systems: a better understanding of their sustainability. Renew Energy 2016;85:1328–33.
[45] Wang J, Chen Y, Dou C, Gao Y, Zhao Z. Adjustable performance analysis of combined cooling heating and power system integrated with ground source heat pump. Energy 2018;163:475–89.
[46] Skorek-Osikowska A, Bartela Ł, Kotowicz J, Sobolewski A, Iluk T, Remiorz L. The influence of the size of the CHP (combined heat and power) system integrated with a biomass fueled gas generator and piston engine on the thermodynamic and economic effectiveness of electricity and heat generation. Energy 2014;67:328–40.
[47] Wang J, Wu J. Investigation of a mixed effect absorption chiller powered by jacket water and exhaust gas waste heat of internal combustion engine. Int J Refrig 2015;50:193–206.
[48] Wang J, Yang Y. Energy, exergy and environmental analysis of a hybrid combined cooling heating and power system utilizing biomass and solar energy. Energy Convers Manag 2016;124:566–77.
[49] Chao L. The study of the solar storage system in the cold Northwest region. Huhehaote: Inner Mongolia University of Technology 2005.
[50] Cong XU, Liu T, Sui J, Liu Q. Evaluation method for energy saving ratio of distributed energy system with multi-energy thermal complementarity. Autom Electr Power Syst 2018;42(4):1–7.
[51] F-Chart. Software, engineering equation solver (EES). http://wwwfchartcom/ees/; 2012.
[52] DdgiT U. Building environmental system simulation and analysis-DeST. Beijing: China Architecture & Building Press; 2006.
[53] Wang J, Zhai Z, Jing Y, Zhang C. Influence analysis of building types and climate zones on energetic, economic and environmental performances of BCHP systems. Appl Energy 2011;88(9):3097–112.
[54] Matuska T, Sourek B, Jirka V, Pokorny N. Glazed PVT collector with polysiloxane encapsulation of PV cells: performance and economic analysis. Int J Photoenergy 2015;2015:1–7.
[55] Wang J, Lu Y, Yang Y, Mao T. Thermodynamic performance analysis and optimization of a solar-assisted combined cooling, heating and power system. Energy 2016;115:49–59.